Spin-vibron coupling effects in single-molecule magnets grafted to a nanoelectromechanical system

V. Moldoveanu and R. Dragomir
National Institute of Materials Physics, Atomistilor 405A, Magurele 077125, Romania

(Received 7 June 2021; revised 26 July 2021; accepted 12 August 2021; published 23 August 2021)

We present a theoretical analysis of the interplay between the spin-vibron and electron-vibron interactions in a hybrid system made of a single-molecule magnet and a suspended conductor. The latter is coupled to particle reservoirs and supports quantized vibrational modes which, once activated, interact with the localized magnetic moment S of the nanomagnet. The dynamics of the molecular spin, the average vibron number, and the transient currents are calculated from the reduced density operator of the hybrid system. We focus on the effect of the vibron-assisted transitions from the lowest energy spin doublet $S_z = \pm S$ to higher energy excited states. The numerical simulations performed for the simplest case $S = 2$ prove that the vibron-assisted spin transitions and dynamics can be described in terms of a three-level Λ model borrowed from quantum optics. In particular we predict the existence of Rabi oscillations of the transient currents as fingerprints of the spin-vibron coupling. The role of symmetric or asymmetric bias configurations in setting different mixtures of molecular spin states in the steady-state regime is also emphasized.

DOI: 10.1103/PhysRevB.104.075441

I. INTRODUCTION

The considerable amount of experimental and theoretical studies on molecular or artificial nanomagnets [1,2] reveal a complex behavior of their localized magnetic moment in the presence of transverse anisotropy, exchange interaction with itinerant electrons, and vibrational degrees of freedom. Quantum tunneling of magnetization (QTM) [3], electrically induced spin switching [4,5], and Franck-Condon blockade [6,7] are nowadays extensively used to characterize various molecular devices [8] and to probe transverse magnetic anisotropy [9].

The localized spin of single-molecule magnets connected to source and drain contacts can be operated only via its exchange interaction with electrons tunneling through the lowest unoccupied molecular orbital (LUMO) [10–12]. In turn, the spin and charge conserving electron-vibron interaction allows the vibrational cooling of suspended nanoresonators [13,14]. Efficient molecular spintronic devices are however expected to allow for *multiple* knobs on both spin and vibrational degrees of freedom.

Such a task can be fulfilled in nanoelectromechanical systems (NEMS) containing a nanomagnet [15,16]. Indeed, the spin-dependent energy terms of the crystal field Hamiltonian acquire some corrections as the anisotropy axes of the nanomagnet follow the deformations of the crystal lattice [1] or the mechanical degrees of freedom of torsional resonators [17]. This spin-mechanical interaction activates vibron-mediated transitions between different states of the localized spin. On the other hand, the vibrational modes of the nanoresonator induce a backaction effect on its electronic transport properties [18,19].

To test this mechanism Ganzhorn *et al.* [20,21] grafted a TbPc2 single molecule to a suspended carbon nanotube (CNT). When coupled to source and drain reservoirs the latter acts as a NEMS and supports various vibrational modes [22–25]. In the experiment presented in Ref. [20] the single-molecule magnet (SMM) spin is first reversed from $-S$ to S by sweeping a magnetic field along the easy-magnetization axis. Then it is found that the direct transitions (DT) which bring the SMM back to its ground state match the frequency of the longitudinal stretching modes (LSM) of the nanotube. This result establishes the existence of spin-vibron coupling in SMM-nanomechanical devices and points to the quantum analog of the Einstein de Haas effect [26].

Theoretical models describing the spin-mechanical interaction in freely rotating nanomagnets or torsional resonators were introduced in a series of papers by Chudnovski and coworkers [27–31]. The considered nanomagnets were closed (i.e., not submitted to electron tunneling from particle reservoirs) and described by an effective Hamiltonian which takes into account the two lowest energy spin components $S_z = \pm S$. This assumption is valid for large anisotropy parameter D which renders higher energy spin components $|S_z| < S$ inactive. For light nanomagnets it is shown that the rotational energy exceeds the energy transferred from the spin tunneling and the latter is frozen. It was also predicted that the magnetization reversal of a single-molecule magnet induces oscillations of a torsional resonator to which it is rigidly coupled.

On the other hand, the theoretical investigation of *open* SMM devices in the presence of both spin-vibron and electron-vibron couplings is still in an incipient stage. May *et al.* [32] studied the vibration-induced Kondo effect in a SMM strongly coupled to the leads. Brüggemann *et al.* [33] investigated the magnetomechanical effects in a magnetic quantum dot. More recently, Kenawy *et al.* [34] presented transport calculations for an $S = 1$ molecule and emphasized

the renormalization of the transverse anisotropy parameter and the changes of the differential conductance due to the spin-vibron interaction. Let us emphasize that these studies were mostly focused on transport properties of SMMs *directly* coupled to the leads. Therefore, the localized spin simultaneously interact with the itinerant electrons and mechanical modes of the SMM.

Instead, the spin dynamics of a nanomagnet interacting with vibrational modes supported by a hosting conducting nanoresonator has not received considerable attention so far. In particular, it would be useful to analyze the time-dependent evolution and the mixing of molecular states when a vibron-assisted current passes through the NEMS.

In the present work we employ a master equation approach to electronic transport and vibron-assisted spin transitions in such hybrid SMM-nanoresonator systems. We investigate the role of excited molecular states by performing time-dependent transport calculations beyond the lowest energy doublet $S_z = \pm S$ for different bias configurations. We identify the role of electron tunneling in triggering the spin-vibron interaction and we provide a detailed discussion on the vibron-assisted spin transitions. The paper is organized as follows: the model and the vibron-assisted transport setting are presented in Sec. II, the numerical results are discussed in Sec. III, and the conclusions are left to Sec. IV.

II. FORMALISM

A. Model and the transport setting

We consider a single-molecule magnet of spin S attached to a suspended nanoelectromechanical structure (e.g., a carbon nanotube) which is coupled to two particle reservoirs. The easy-axis magnetization z is assumed to be perpendicular to the direction of the electronic flow. The Hamiltonian of the hybrid system reads

$$H_{\rm hyb} = H_{\rm hyb,0} + H_{\rm sp\text{-}vb} + H_{\rm el\text{-}vb}, \tag{1}$$

where $H_{\rm hyb,0}$ stands for the "free" Hamiltonian of disentangled subsystems (i.e., the conducting nanoresonator and the attached SMM) and the last two terms represent the spin-vibron coupling and the electron-vibron interaction. Specifically we have

$$H_{\rm hyb,0} = -D\hat{S}_z^2 + E\left(\hat{S}_x^2 - \hat{S}_y^2\right) + g\mu_B B\hat{S}_z + \hbar\omega_0 a^\dagger a + \sum_\sigma \epsilon_\sigma c_\sigma^\dagger c_\sigma + U\hat{n}_\uparrow\hat{n}_\downarrow + g\mu_B B\hat{s}_z. \tag{2}$$

The first two terms in Eq. (2) correspond to the crystal field Hamiltonian of the SMM, with the easy-axis and transverse anisotropy coefficients D and E. The identity $\hat{S}_x^2 - \hat{S}_y^2 = (\hat{S}_+^2 + \hat{S}_-^2)/2$ shows that the transverse anisotropy component induces quantum tunneling of magnetization through the jump operators $\hat{S}_\pm$. The quantized vibrational mode of frequency ω_0 is described by harmonic oscillator operators a, $a^\dagger$.

The last three terms of $H_{\rm hyb,0}$ describe the suspended subsystem. To keep the model simple we assume that the transport is only due to the spin-degenerate lowest energy level $\epsilon_\uparrow = \epsilon_\downarrow := \epsilon_0$, with $c_\sigma^\dagger/c_\sigma$ being the corresponding creation/annihilation operators. $\hat{n}_\sigma = c_\sigma^\dagger c_\sigma$ is the number operator for electronic spin σ and U is the strength of the Coulomb interaction. The two Zeeman energy terms are due to a constant magnetic field $\mathbf{B} = B\mathbf{e}_z$ applied along the z axis. $(\hat{s})$ is the electronic spin operator and μ_B and g are the Bohr magneton and the Landé factor.

The spin-vibron coupling $H_{\rm sp\text{-}vb}$ is associated to the change of the anisotropy axes as a response to mechanical vibrations. Assuming as in Ref. [20] that the longitudinal modes of the CNT induce a rotation of angle φ of the SMM around the z axis one can write the rotation vector as $\mathbf{\Omega} = \varphi\mathbf{e}_z$. Then the easy-axis anisotropy contribution $D\hat{S}_z^2$ is left invariant by the transformation $\mathbf{e}_z \to \mathbf{e}_Z = \mathbf{e}_z + \mathbf{\Omega}\times\mathbf{e}_z$, whereas the changes of the transverse axes add up to a supplementary term $2E\{\hat{S}_x, \hat{S}_y\}\varphi$. As the nanoresonator modes are quantized, φ is expressed in terms of creation and annihilation operators [35]:

$$\varphi = \sqrt{\frac{\hbar}{2I_z\omega_0}}(a^\dagger + a), \tag{3}$$

where we introduced the dimensionless parameter $\alpha = \sqrt{\hbar/2I_z\omega_0}$ and I_z is the inertia moment of the molecular nanomagnet. Then the spin-vibron Hamiltonian reads as (see, e.g., Ref. [17])

$$H_{\rm sp\text{-}vb} = -i\alpha E(\hat{S}_+^2 - \hat{S}_-^2)(a^\dagger + a). \tag{4}$$

Finally, the electron-vibron coupling of strength λ is given by

$$H_{\rm el\text{-}vb} = \lambda\sum_\sigma c_\sigma^\dagger c_\sigma(a^\dagger + a). \tag{5}$$

In the absence of the transverse anisotropy (i.e., for $E = 0$) the states of the Hamiltonian $H_{\rm hyb,0}$ are labeled by four quantum numbers: the electronic occupation number Q, that is the eigenvalue of the total charge operator $\hat{Q} = e\sum_\sigma c_\sigma^\dagger c_\sigma$, the electronic spin projection $\sigma = \uparrow, \downarrow$, the molecular spin projection S_z defined by $\hat{S}_z|S_z\rangle = S_z|S_z\rangle$, and the vibron number N. These quantum numbers describe a basis whose elements are $\{|0, 0, S_z, N\rangle\}$, $\{|1, \sigma, S_z, N\rangle\}$, and $\{|2, 0, S_z, N\rangle\}$. The N-vibron states $|N\rangle$ are defined by $a^\dagger a|N\rangle = N|N\rangle$.

If $E \neq 0$ the projection S_z of the molecular spin is no longer conserved, whereas Q and σ can still be used to label the eigenfunctions of $H_{\rm hyb,0}$. For further use let us explicitly write the "empty" ($Q = 0$) and "single-charged" ($Q = 1$) eigenfunctions with respect to the basis $|Q, \sigma, S_z, N\rangle$ (here $\nu = 1, \ldots, 2S + 1$):

$$|\phi_{0,\nu}; N\rangle = \sum_{S_z} A_{S_z}^{(\nu)}|0, 0, S_z, N\rangle, \tag{6}$$

$$|\phi_{\sigma,\nu}; N\rangle = \sum_{S_z} B_{\sigma S_z}^{(\nu)}|1, \sigma, S_z, N\rangle. \tag{7}$$

The two-electron states ($Q = 2$) will not be needed in our calculations since we assume that double occupancy of the suspended system is forbidden due to the strong Coulomb interaction U. Then the relevant states are $\{|\phi_{p,\nu}; N\rangle\}$, where the index $p = \{0, \sigma = \uparrow, \downarrow\}$ indicates the occupation charge and the electronic spin of a given state ν of the hybrid system.

The electron-vibron coupling is diagonalized via the unitary Lang-Firsov transformation $U_{LF} = e^{\lambda/\hbar\omega_0\hat{N}_S(a^\dagger - a)}$, where $\hat{N}_S = \sum_\sigma c_\sigma^\dagger c_\sigma$. The transformed Hamiltonian of the hybrid system becomes

$$\tilde{H}_{\rm hyb} = \tilde{H}_{\rm hyb,0} + H_{\rm sp\text{-}vb} + 2i\alpha\lambda E(\hat{S}_+^2 - \hat{S}_-^2)\hat{N}_S, \tag{8}$$

where we introduced $\tilde{H}_{\rm hyb,0} = H_{\rm hyb,0} - \lambda^2\hat{N}_S/\hbar\omega_0$.

Note that the eigenfunctions of $\tilde{H}_{\rm hyb,0}$ are still given by Eqs. (6) and (7). The corresponding eigenvalues $\mathcal{E}^{(0)}_{p,\nu,N}$ are defined by the identity $\tilde{H}_{\rm hyb,0}|\phi_{p,\nu};N\rangle = \mathcal{E}^{(0)}_{p,\nu,N}|\phi_{p,\nu};N\rangle$ and can be written in the form

$$\mathcal{E}^{(0)}_{p,\nu,N} = E_{p,\nu} + N\hbar\omega_0, \tag{9}$$

where $E_{p,\nu}$ is an eigenvalue of $\tilde{H}_{\rm hyb,0} - \hbar\omega_0 a^\dagger a$. Let us note that a Lang-Firsov transformation which eliminates the spin-vibron interaction is not generally available. A particular case where this is still possible imposes the condition $S \leqslant 1$ on the molecular spin [34].

The full Hamiltonian $\tilde{H}_{\rm hyb}$ is also diagonalized numerically and its eigenstates acquire a dressed-state structure:

$$\left|\psi^{(p)}_j\right\rangle = \sum_{\nu,N} \mathcal{C}^{(p)}_{j,\nu,N}|\phi_{p,\nu};N\rangle, \tag{10}$$

where $j = 1,\ldots(2S+1)N_0$ and N_0 is the number of Fock states considered in the numerical diagonalization procedure. Note that these dressed states can still be labeled by the charge and spin occupation index p. On the other hand, we find that if $\alpha E \ll \lambda$ the eigenvalues $\mathcal{E}^{(p)}_j$ of $\tilde{H}_{\rm hyb}$ are to a very good extent given by the eigenvalues of $\tilde{H}_{\rm hyb,0}$.

Assuming a lattice model for the two [left (L) and right (R)] semi-infinite leads coupled to the suspended nanosystem the corresponding tunneling Hamiltonian becomes

$$H_T(t) = \sum_{\alpha=L,R}\sum_{\sigma}\int_0^\pi dq_\alpha \chi_\alpha(t)(V^\alpha_\sigma c^\dagger_\sigma c_{q_\alpha\sigma} + \text{H.c.}), \tag{11}$$

where V^α_σ is the hopping amplitude between the level ϵ_σ and the electronic spin states in the lead α. Here q stands for the electronic momentum on the leads and $\varepsilon_q = 2t_L\cos q$ is the energy of the incident electron (with t_L being the hopping constant on the leads).

The functions $\chi_\alpha(t)$ ($\alpha = L, R$) simulate the switching of the contacts between the suspended system and the leads. In this work we consider that the coupling to the leads is established at the instant $t = 0$ and that $\chi_{L,R}(t) = \theta(t)$, where $\theta(x)$ is the step function. The spin polarizations of the leads is defined as $P^\alpha := (\Gamma^\alpha_\uparrow - \Gamma^\alpha_\downarrow)/(\Gamma^\alpha_\uparrow + \Gamma^\alpha_\downarrow)$ (see [12]).

The LF transformation also acts on the fermionic operator of the suspended system which now becomes

$$\tilde{c}_\sigma = c_\sigma e^{-\lambda(a^\dagger - a)/\hbar\omega_0} := c_\sigma\hat{\Lambda}. \tag{12}$$

Then the matrix elements of the transformed tunneling Hamiltonian $\tilde{H}_T$ with respect to the basis $\{|\phi_{p,\nu};N\rangle\}$ contain the Franck-Condon factors:

$$\langle N|\hat{\Lambda}|N'\rangle = e^{-q_0^2/4}\sqrt{\frac{N_<!}{N_>!}}\left(\frac{q_0}{\sqrt{2}}\right)^{|N-N'|} \times \text{sgn}(N'-N)^{|N-N'|}L^{|N'-N|}_{N_<}\left(q_0^2/2\right),$$

where $q_0 = \sqrt{2}\lambda/\hbar\omega_0$, $L^n_m(x)$ are the generalized Laguerre polynomials, and we introduced $N_< = \min\{N, N'\}$, $N_> = \max\{N, N'\}$.

Collecting all the terms one writes the Hamiltonian of the open hybrid system as

$$H = \tilde{H}_{\rm hyb} + H_{\rm leads} + \tilde{H}_T, \tag{13}$$

where $H_{\rm leads}$ describes the noninteracting particle reservoirs and is not changed by the LF transformation.

Standard calculations performed within the Markov approximation provide the master equation for the reduced density operator (RDO) ρ of the hybrid system:

$$\dot{\rho}(t) = -\frac{i}{\hbar}[\tilde{H}_{\rm hyb}, \rho(t)] - \mathcal{L}_{\rm leads}[\rho(t)] - \mathcal{L}_\kappa[\rho(t)], \tag{14}$$

where $\mathcal{L}_{\rm leads}$ takes into account the contribution of the particle reservoirs (i.e., the leads) and acquires the form (H.c. stands for Hermitian conjugate)

$$\mathcal{L}_{\rm leads}[\rho(t)] = \frac{\pi}{\hbar}\left(\sum_{\alpha,\sigma}[\mathcal{A}_{\alpha\sigma}, \mathcal{B}_{\alpha\sigma}\rho(t) - \rho(t)\mathcal{D}^\dagger_{\alpha\sigma}] + \text{H.c.}\right).$$

In the basis of dressed states $|\psi^{(p)}_j\rangle$ the operators $\mathcal{A}$, $\mathcal{B}$, and $\mathcal{D}$ are given as follows:

$$\mathcal{A}_{\alpha\sigma} = \sum_{jp,j'p'} T^{\alpha\sigma}_{jp,j'p'}\left|\psi^{(p)}_j\right\rangle\left\langle\psi^{(p')}_{j'}\right|, \tag{15}$$

$$\mathcal{B}_{\alpha\sigma} = \sum_{ir,i'r'} \overline{f}_\alpha\left(\mathcal{E}^{(r')}_{i'} - \mathcal{E}^{(r)}_i\right)\overline{T}^{\alpha\sigma}_{i'r',ir}\left|\psi^{(r)}_i\right\rangle\left\langle\psi^{(r')}_{i'}\right|, \tag{16}$$

$$\mathcal{D}_{\alpha\sigma} = \sum_{ir,i'r'} f_\alpha\left(\mathcal{E}^{(r)}_i - \mathcal{E}^{(r')}_{i'}\right)T^{\alpha\sigma}_{ir,i'r'}\left|\psi^{(r)}_i\right\rangle\left\langle\psi^{(r')}_{i'}\right|, \tag{17}$$

where $f_\alpha(E)$ is the Fermi function of the lead α and we introduced the notation $\overline{f}_\alpha(E) = 1 - f_\alpha(E)$ and the jump operators between pairs of fully interacting states ($D_{\alpha\sigma}$ is the density of states of the lead α):

$$T^{\alpha\sigma}_{jp,j'p'} = \sqrt{D_{\alpha\sigma}}V^\alpha_\sigma\left\langle\psi^{(p)}_j\right|c^\dagger_\sigma\hat{\Lambda}^\dagger\left|\psi^{(p')}_{j'}\right\rangle. \tag{18}$$

For completeness we also included in the master equation the dissipation processes due to a thermal reservoir described by the Bose-Einstein distribution n_B and temperature T. Under the Lang-Firsov transformation the corresponding Lindblad term $\mathcal{L}_\kappa$ reads as [36]

$$\mathcal{L}_\kappa\rho(t) = (n_B+1)\mathcal{D}_\kappa[a]\rho(t) + n_B\mathcal{D}_\kappa[a^\dagger]\rho(t) + \left(\frac{\lambda}{\hbar\omega_0}\right)^2(2n_B+1)\mathcal{D}_\kappa[\hat{N}_S]\rho(t), \tag{19}$$

where we introduced the notation

$$\mathcal{D}_\kappa[X]\rho(t) = \frac{\kappa}{2}(X^\dagger X\rho + \rho X^\dagger X - 2X\rho X^\dagger). \tag{20}$$

The master equation must be solved with respect to the basis of fully interacting states $\{\psi^{(p)}_j\}$. However, for the sake of a more intuitive discussion of the vibron-assisted transitions we shall discuss the time dependence of the RDO in terms of disentangled basis $\{|\phi_{p,\nu};N\rangle\}$ by using the unitary transformation which connects it to the dressed states basis.

The occupation of a given configuration $|\phi_{p,\nu}\rangle$ of the hybrid system is obtained by summing the populations of the N-vibron states:

$$P_{0,\nu} = \sum_N\langle\phi_{0,\nu};N|\rho(t)|\phi_{0,\nu};N\rangle, \tag{21}$$

$$P_{1,\nu} = \sum_{N,\sigma}\langle\phi_{\sigma,\nu};N|\rho(t)|\phi_{\sigma,\nu};N\rangle. \tag{22}$$

Note that $P_{1,\nu}$ collects the occupation of electronic states with both spin orientations $\sigma = \uparrow, \downarrow$. The statistical average of the

localized spin is calculated as

$$\langle S_z\rangle(t) = \mathrm{Tr}\{\rho(t)\hat{S}_z\}, \tag{23}$$

where the trace is taken over all states of the hybrid system. Similarly one can compute the average number of vibrons $\langle N_v\rangle(t) := \mathrm{Tr}\{\rho(t)a^\dagger a\}$ and the total electronic charge.

The time-dependent currents follow from the continuity equation of the charge occupation $\mathcal{Q}_S = e\hat{N}_S$ of the hybrid system (e denotes the electron charge):

$$\frac{d}{dt}\mathcal{Q}_S(t) = e\,\mathrm{Tr}\left\{\hat{N}_S\frac{d}{dt}\rho(t)\right\} = J_L(t) - J_R(t). \tag{24}$$

B. Vibron-assisted molecular transitions

In this subsection we describe in some detail the transitions experienced by the molecular spin in the presence of vibron-assisted tunneling. The spin-vibron coupling [see Eq. (4)] conserves both the charge occupation Q and the electronic spin σ; hence its nonvanishing matrix elements are of the form $\langle\phi_{p,\nu};N|H_{\text{sp-vb}}|\phi_{p,\nu'};N'\rangle$, where $|N-N'|=1$. The spin "delocalization" of a state $|\phi_{p,\nu};N\rangle$ over more components $|S_z\rangle$ with the same parity is controlled by the coefficients $A^{(\nu)}_{S_z}$ and $B^{(\nu)}_{S_z}$ in Eqs. (6) and (7).

However, if the magnetic field is chosen away from the degeneracy points $B = -D(S_z + S_z')/g\mu_B$ of the energies associated to the pair of states $|S_z\rangle$ and $|S_z'\rangle$, one can identify a majoritary spin component $\overline{S}_z$ such that $|A^{(\nu)}_{\overline{S}_z}|^2 \gg |A^{(\nu)}_{S_z}|^2$ for all the remaining projections $S_z \neq \overline{S}_z$. A similar argument holds for pairs of single-charged states $|\phi_{\sigma,\nu}\rangle$. These majoritary components $\overline{S}_z$ are found from the exact diagonalization of $\tilde{H}_{\text{hyb},0}$ and allow us to switch to the more intuitive notation $|\phi_{p,\nu}\rangle \to |\phi_{p,\overline{S}_z}\rangle$; we shall also use the correspondence $E_{p,\nu} \to E_{p,\overline{S}_z}$.

To be more specific, let us consider the nanomagnet of spin $S=2$ which we shall investigate in the next section. The vibron-assisted transition associated to the lowest energy spin doublet $\overline{S}_z = \pm 2$ involves the states $|\phi_{p,-2};N+1\rangle$ and $|\phi_{p,2};N\rangle$. If $E \ll D$ the resonant frequency is well approximated by $\hbar\omega_0 = 4g\mu_B B$. Note that the matrix element $\langle\phi_{p,2}|\hat{S}_+^2|\phi_{p,-2}\rangle$ is small, as the jump operators couple the dominant component $\overline{S}_z = \pm 2$ of one state to the minoritary component $\overline{S}_z = 0$ of the other. On the other hand, the higher energy state $|\phi_{p,0};N\rangle$ couples strongly to $|\phi_{p,\pm 2};N+1\rangle$ because the dominant components obey the condition $\Delta S_z = \pm 2$.

It is not difficult to see that the single-electron eigenvalues $E_{\sigma,\overline{S}_z}$ that participate to vibron-assisted transitions are arranged in a spin-split Λ-type configuration (see the sketch in Fig. 1). A similar simpler configuration describes the spin-vibron transitions between the "empty" states $|\phi_{0,0};N\rangle$ and $|\phi_{0,\pm 2};N\rangle$. The spin transitions corresponding to these spectral structures resemble the ones associated to the three-level model from quantum optics [37]. The resonant frequencies associated to each "branch" of the Λ configuration are approximatively given by

$$\hbar\omega_\pm = 4D \mp 2g\mu_B B, \tag{25}$$

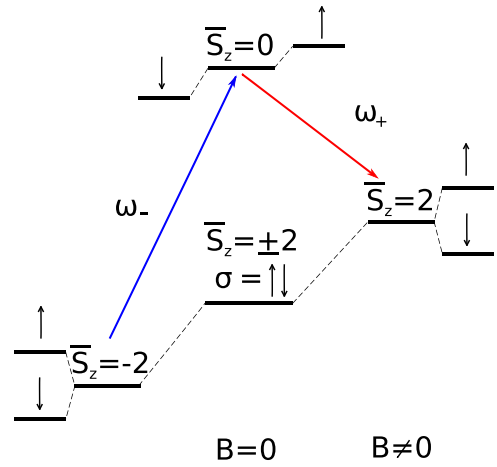

FIG. 1. Spin-split Λ-type configuration of the single-particle states of the $S=2$ hybrid system. The horizontal solid lines represent energy levels of the hybrid system alone (i.e., without vibrons) and the arrows indicate the vibron-assisted transitions between states with dominant spin components $\overline{S}_z = 0$ and $\overline{S}_z = \pm 2$. The resonant frequencies are $\omega_\pm$. If $\omega_0 = \omega_-$ the blue/red arrows mark the resonant/off-resonant transitions.

and do not depend on σ such that the spin up and down states contribute simultaneously to the transitions. More importantly, the detuning $\omega_- - \omega_+ = 4g\mu_B B$ is much smaller than both frequencies $\omega_\pm$. This means that one cannot reduce the dynamics of the hybrid system to a single pair of resonant states (e.g., $\overline{S}_z = \{0,-2\}$ for $\omega_0 = \omega_-$) while disregarding the pair $\overline{S}_z = \{0,2\}$ as inactive or "dark." Therefore, a more appropriate picture must involve two "excitation/relaxation" paths for the vibrons, with one being resonant and the other slightly off-resonant (see the arrows in Fig. 1). As we shall see below, this regime provides important insight on the vibron-assisted processes, both in the short and long time range.

Supposing that the system is initially set in the state $|\phi_{0,\overline{S}_z=-2};N=0\rangle$ which does not contain electrons or vibrons, one can still rely on the tunneling processes to drive the vibron-absorbing transitions $|\phi_{p,-2};N+1\rangle \to |\phi_{p,0};N\rangle$. Indeed, vibrons can be generated in the system by properly setting the chemical potentials of the source and drain leads [38]. By analyzing the dissipative terms contained in Eqs. (16) and (17) one infers that if $\mu_L > \mathcal{E}_{\sigma,\overline{S}_z,N'} - \mathcal{E}_{0,\overline{S}_z,N} = \tilde{\epsilon}_\sigma + (N'-N)\hbar\omega_0$, the tunneling processes from the left lead increase the number of vibrons by $N'-N$. Similarly, the case $N' < N$ corresponds to vibron absorption. Here we introduced the renormalized single-particle energy $\tilde{\epsilon}_\sigma = \epsilon_0 - \lambda^2/\hbar\omega_0 - g\mu_B B s_z$, where the second term is the energy shift due to the Lang-Firsov transform and the third term counts the Zeeman energy of the electronic spin $s_z = \pm 1/2$. Also, when $\mu_R < \mathcal{E}_{\sigma,\overline{S}_z,N'} - \mathcal{E}_{0,\overline{S}_z,N}$ and $N' < N$ the tunneling out processes leave the system in the excited state containing $N-N'$ vibrons. Based on these observations we introduce the particular chemical potentials

$$\mu_{\text{in/out}}(l) = \tilde{\epsilon}_\sigma \pm \frac{2l+1}{2}\hbar\omega_0, \tag{26}$$

which are associated to the emission of l vibrons when electrons tunnel into or from the system.

Now let us introduce three bias configurations which allow specific classes of vibron-assisted tunneling processes. The *symmetric* bias configuration (henceforth named $B_{\rm sym}$) is realized if the chemical potentials are tuned such that $\mu_L = \mu_{\rm in}(N_0)$ and $\mu_R = \mu_{\rm out}(N_0)$, where N_0 is the maximum number of vibrons allowed in the numerical simulations. The first condition on μ_L means that the tunneling-in processes lead to occupation of vibrationally excited states $|\phi_{\sigma,\bar{S}_z}; N \leqslant N_0\rangle$. The second condition for μ_R implies that the tunneling-out processes allow the population of vibrationally excited states $|\phi_{0,\bar{S}_z}; N\rangle$.

One can also consider two *asymmetric* bias configurations $B_{\rm out}$ and $B_{\rm in}$. The configuration $B_{\rm out}$ only allows vibron emission via tunneling-out processes, by lowering the chemical potential of the source lead to $\mu_L = \mu_{\rm in}(0)$ and keeping $\mu_R = \mu_{\rm out}(N_0)$. In contrast, in the setup $B_{\rm in}$ the tunneling-out processes cannot lead to vibron emission as we tune $\mu_R = \mu_{\rm out}(0)$ while $\mu_L = \mu_{\rm in}(N_0)$.

III. NUMERICAL RESULTS AND DISCUSSION

In this section we present transport calculations for a hybrid system containing a localized spin $S = 2$. This simple model already reveals the physics associated to transitions beyond the lowest energy spin doublet $S_z = \pm S$. Larger values of S could be also considered, at the expense of more involved numerical calculation and more complicated spectral configurations. The easy-axis anisotropy coefficient is $D = 0.056$ meV, the strength of the electron-vibron coupling is $\lambda = 0.2$ meV, and the magnetic field is set to $B = 150$ mT. For the lowest single-particle energy of the electronic system we used $\epsilon_\uparrow = \epsilon_\downarrow := \epsilon_0 = 0.5$ meV. The loss coefficient is $\kappa = 0.05$ μeV and the temperature of the environment $T = 50$ mK. Let us note that our parameters are such that $\lambda/\hbar\omega_0 < 1$ and the spin-vibron coupling strength $\alpha E \ll \lambda$. Further discussion on the parameters used in the numerical simulations will be given at the end of this section.

By diagonalizing the Hamiltonian of the hybrid system at $\alpha = 0$ we find that the resonant frequency for transitions between the states with majoritary molecular spin $S_z = \{0, -2\}$ is $\hbar\omega_- = 0.27$ meV. Also, the transitions between states having $S_z = \{0, 2\}$ correspond to $\hbar\omega_+ = 0.2$ meV.

The master equation (14) is solved by choosing the initial state of the system as $|\phi_{0,\bar{S}_z=-2}; 0\rangle$. For the simplicity of writing we shall henceforth use the simplified notation $\bar{S}_z \to S_z$ for the dominant spin components of a given state. As we neglect the exchange interaction between the electrons passing through the suspended system and the localized spin, the states with dominant spin components $S_z = \pm 1$ will not significantly contribute to transport. The convergence of the numerical transport simulations was obtained by taking into account up to $N_0 = 5$ vibrons, while the numerical diagonalization is performed using up to 25 vibron states. The time evolution of the average spin $\langle S_z\rangle$ is given in Fig. 2 for the three bias configurations introduced in Sec. II B and for both resonant frequencies $\omega_\pm$ corresponding to the two "branches" of the Λ configuration. The effect of the spin-vibron coupling is confirmed by the increase of the average molecular spin from its initial value $\langle S_z\rangle(t = 0) = -2$ as the current passes through the system. Figures 2(a) and 2(b) reveal that in the stationary regime the average spin converges to roughly the same value $\langle S_z\rangle = 0$, irrespective of the resonant path set by the frequencies $\omega_\pm$. We also discern two time scales of the spin evolution. In the resonant regime $\omega_0 = \omega_-$ corresponding to the left branch of the Λ configuration the spin increases abruptly in just a few nanoseconds [see Fig. 2(a)], especially for the symmetric bias case $B_{\rm sym}$. Around $t = 10$ ns the system enters a second regime in which the increase of $\langle S_z\rangle$ slows down and it takes at least tens of nanoseconds until it approaches the stationary state. In the asymmetric configurations $B_{\rm out}$ and $B_{\rm in}$ the spin changes even more and the stationary regime is achieved only around $t \approx 150$ ns.

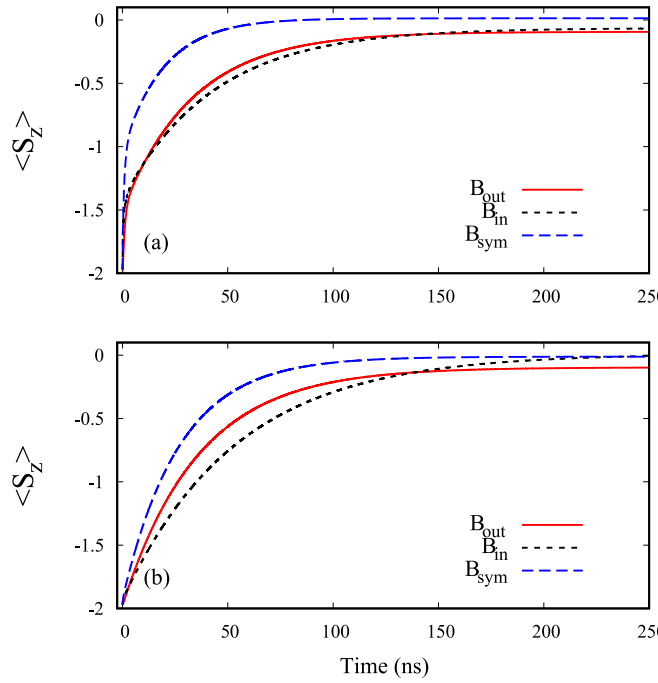

FIG. 2. Dynamics of the average molecular spin for both resonant frequencies $\omega_\pm$ in the symmetric and asymmetric bias configurations. (a) $\omega_0 = \omega_-$; (b) $\omega_0 = \omega_+$. The chemical potentials are as follows: $\mu_L = 0.485$ meV, $\mu_R = -0.6$ meV for the configuration $B_{\rm out}$, $\mu_L = 1.3$ meV, $\mu_R = 0.2$ meV for $B_{\rm in}$, and $\mu_L = 1.3$ meV, $\mu_R = -0.6$ meV for the symmetric bias $B_{\rm sym}$. Other parameters: $\alpha = 0.15$, $D = 0.056$ meV, $E/D = 1/5$, and $V_L = V_R = 15$ μeV. The leads are not spin-polarized.

In the resonant case $\omega_0 = \omega_+$ [see Fig. 2(b)] the separation between the two time scales is less obvious. Indeed, the sudden spin increase at short times is replaced by a rather smooth evolution.

Figure 2 reveals that the molecular spin dynamics depends *both* on the bias configuration and on the resonant conditions for vibron-assisted transitions. It also shows that the fastest operation on the molecular spin is obtained by setting the system in the symmetric bias configuration and the frequency $\omega_0 = \omega_-$.

The detailed features of the short time dynamics for the asymmetric bias configuration $B_{\rm in}$ for both resonant frequencies are presented in Fig. 3(a) (the other configurations lead to similar results). For $\omega_0 = \omega_-$ the average spin $\langle S_z\rangle$ displays periodic oscillations which are washed out at large times

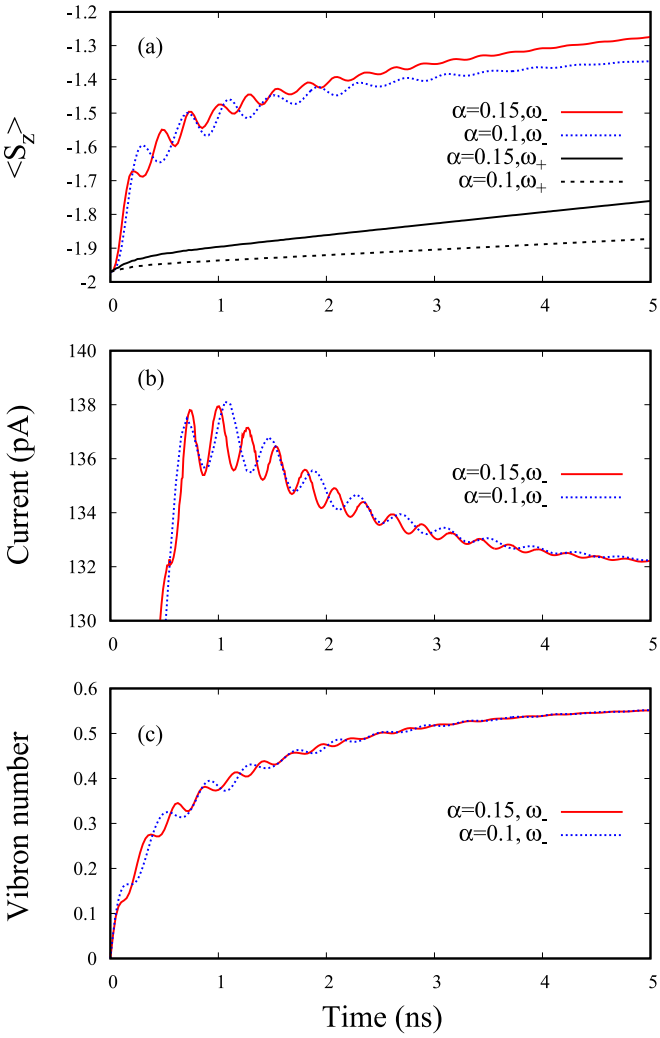

FIG. 3. (a) Short time dynamics of the molecular spin for asymmetric bias configurations $B_{\rm in}$ at both resonant frequencies $\omega_0 = \omega_\pm$. The period of the oscillations depends on α. (b) Rabi-like oscillations of the transient current J_R in the drain lead for two values of the spin-vibron coupling in the $B_{\rm in}$ configuration. (c) The average vibron number. The initial state is $|\phi_{0,-2};0\rangle$. Other parameters: $\mu_L = 1.3$ meV, $\mu_R = 0.2$ meV, $D = 0.056$ meV, $E/D = 1/5$, and $V_L = V_R = 15$ μeV.

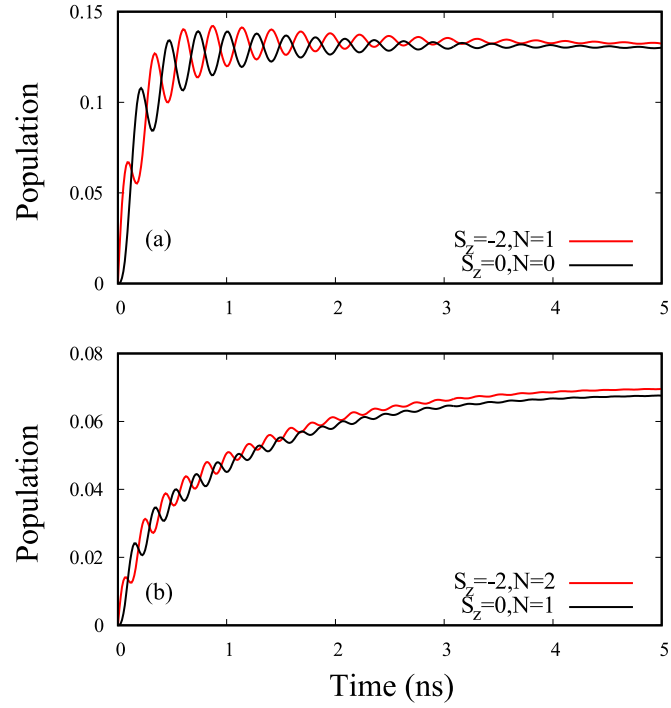

FIG. 4. Short time occupation $P_{Q=1,S_z,N}$ of the lowest energy N-vibron states $|\phi_{Q=1,S_z};N\rangle$ for asymmetric bias configuration $B_{\rm in}$ at resonant frequency $\omega_0 = \omega_-$. (a) $P_{Q=1,-2,1}$ and $P_{Q=1,0,0}$; (b) $P_{Q=1,-2,2}$ and $P_{Q=1,0,1}$. Other parameters: $\alpha = 0.15$, $\mu_{L,\rm in} = 1.3$ meV, $\mu_{R,\rm in} = 0.2$ meV, $D = 0.056$ meV, $E/D = 1/5$, and $V_L = V_R = 15$ μeV.

by the dissipative tunneling processes and thermal damping. These are nothing but the analog of the optical Rabi oscillations encountered in quantum-dot-cavity systems. Here, they correspond to the out-of-phase oscillations of the occupations of states with molecular quantum number $S_z = -2$ and $S_z = 0$. As in the Jaynes-Cummings model of quantum optics, the period of the oscillations increases if the coupling strength α decreases. One also observes that the ω_+ resonant path does not induce Rabi oscillations of the spin. Nonetheless, the increase rate of the average spin clearly depends on α. We find that for smaller spin-vibron coupling the time needed to achieve the stationary state increases considerably.

Figure 3(b) shows that the transient current J_R which is established in the output lead also displays Rabi oscillations. Moreover, the dependence of the oscillations on the spin-vibron coupling α mimics the behavior of the molecular spin shown in Fig. 3(a). From these results one infers that the spin-vibron coupling leaves its fingerprints on *both* the transient current and molecular spin.

For completeness we also calculated the average of the vibron number [see Fig. 3(c)]. It also displays Rabi oscillations whose maxima roughly correspond to the minima of the spin shown in Fig. 3(a) and confirm the scenario of vibron-assisted spin transitions. We also observe that the number of vibrons almost reaches the stationary regime at $t = 5$ ns. We find in fact that for all bias configurations the vibron number does not change anymore after $t = 10$ ns (not shown). This suggests that the behavior of the molecular spin at intermediate and long times is due to the spin-vibron interaction alone.

A more detailed analysis of the vibronic Rabi oscillations observed in the bias configuration $B_{\rm in}$ is provided by the time-dependent occupation of certain states $|\phi_{\sigma,S_z};N\rangle$. In Fig. 4 we present the total occupation of single-electron states $P_{Q=1,S_z,N}(t) = \sum_\sigma \langle\phi_{\sigma,S_z};N|\rho(t)|\phi_{\sigma,S_z};N\rangle$ for $N = 0, 1, 2$. The out-of-phase Rabi oscillations associated to the pairs of states $\{|\phi_{\sigma,-2};N\rangle, |\phi_{\sigma,0};N-1\rangle\}$ are consistent with the resonant spin transitions corresponding to the ω_- branch of the Λ configuration. Moreover, the period of the Rabi oscillations depends on the number of vibrons N, namely it decreases when N increases. In order to explain this fact one has to recall that the matrix elements of the electron-vibron interaction between two pairs of states [see Eq. (4)] have a prefactor $\sqrt{N+1}$, which leads to larger Rabi frequencies for higher vibronic energies. Again, this is the analog of the N-photon Rabi oscillations predicted by the Jaynes-

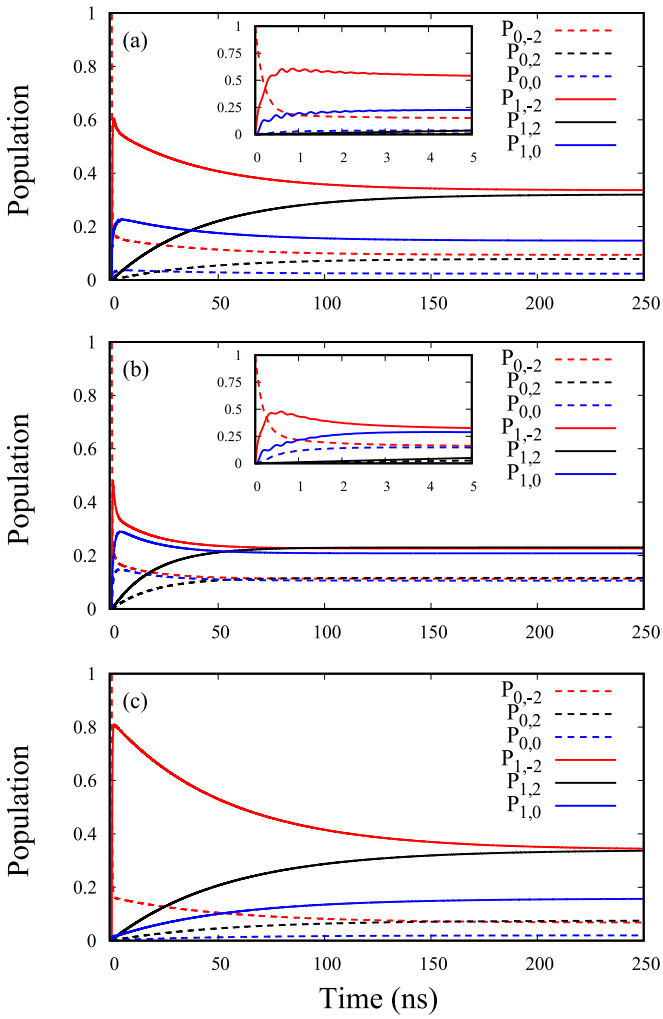

FIG. 5. Time-dependent populations P_{Q,S_z} of empty ($Q = 0$, dashed lines) and single-electron states ($Q = 1$, solid lines) associated to a dominant component S_z of the molecular spin. (a) The asymmetric bias configuration $B_{\rm in}$, $\omega_0 = \omega_-$. (b) The symmetric configuration $B_{\rm sym}$, $\omega_0 = \omega_-$. (c) The asymmetric bias configuration $B_{\rm in}$, $\omega_0 = \omega_+$. In all figures the initial state is $|\phi_{0,-2}; 0\rangle$. Other parameters are the same as in Fig. 2.

Cummings model [39]. The individual populations of the states carrying dominant spin $S_z = 2$ do not display Rabi oscillations (not shown).

Further insight on the long-time behavior and steady-state spin configurations is gained by analyzing the populations associated to a dominant molecular spin S_z. In Fig. 5 we show the populations $P_{0,S_z}/P_{1,S_z}$ of the empty/single-charged states as calculated from Eqs. (21) and (22).

In the asymmetric configuration $B_{\rm in}$ and for $\omega_0 = \omega_-$ [see Fig. 5 (a)] the single-electron excited states having $S_z = 0$ are already populated around $t = 0.25$ ns, which corresponds to the abrupt increase of the molecular spin seen in Fig. 2(a). The transitions leading to these states are resonant (i.e., $\omega_0 = \omega_-$) and associated to the left "branch" of the Λ configuration. The single-electron states contributing to $P_{1,0}$ emerge in the dynamics at earlier times than the empty states contained in $P_{0,0}$, as seen in the inset of Fig. 3(a). This behavior illustrates the mechanism which activates the spin-vibron coupling in the bias configuration $B_{\rm in}$: vibrons are emitted via tunneling-in processes such that the first vibron-assisted transitions involve the "charged" molecular states $|\phi_{\sigma,-2}; N+1\rangle$ and $|\phi_{\sigma,0}; N\rangle$. Nonetheless, the vibron conserving tunneling-out processes also allow the occupation of the vibrationally excited empty states $|\phi_{0,-2}; N+1\rangle$ which then activate the molecular transitions involving the states $|\phi_{0,0}; N\rangle$. The inset of Fig. 5(a) also shows that the vibronic Rabi oscillations observed in the short time behavior of the average molecular spin and transient current are correlated to similar oscillations of the populations $P_{1,-2}$ and $P_{1,0}$.

In contrast, the population $P_{1,2}$ emerges in the dynamics at longer times (around $t \sim 10$ ns) via off-resonant transitions corresponding to the right "branch" in Fig. 1. It is this second type of spin transition which causes the slower increase of the molecular spin towards the steady-state value. By inspecting Fig. 5(a) one notices that at intermediate times the states with the lowest molecular spin $S = -2$ and $S = 0$ are partially depleted while the populations $P_{1,2}$ and $P_{0,2}$ gradually increase. Interestingly, in the long time limit the total weights $P_{1,S_z} + P_{0,S_z}$ of the "antiparallel" spin states $S_z = \pm 2$ are almost equal while the population of the highest energy states is three times smaller (i.e., $P_{1,0} + P_{0,0} \approx 0.16$). One can therefore say that for this bias setup the stationary spin configuration of the SMM is roughly given by the antiparallel spin components $S_z = \pm 2$.

In Fig. 5(b) we present the spin-resolved populations corresponding to the symmetric bias configuration $B_{\rm sym}$ and to the same resonant frequency $\omega_0 = \omega_-$ as in Fig. 5(a). In this regime both the tunneling-in and -out processes allow the generation of vibrons, and we find that the number of vibrons is much larger (not shown). The inset shows a significant contribution of the "empty" molecular states to $P_{0,0}$ in the transient regime. This explains the fastest increase of $\langle S_z \rangle$ in the symmetric configuration [see Fig. 2(a)]. Small Rabi oscillations of $P_{1,-2}$ and $P_{1,0}$ are still noticed in the inset. More importantly, the system ends up in a mixture of states with nearly equal weights for *each* spin orientation. Indeed, in contrast to configuration $B_{\rm in}$, here the occupation of $S_z = 0$ states is considerably enhanced. Note also that the stationary regime is already installed around $t \sim 50$ ns, which is much faster than for the bias configuration $B_{\rm in}$.

Now we briefly discuss the population dynamics in the case $\omega_0 = \omega_+$. Due to the resonant transitions along the right "branch" of the Λ configuration, the depletion of $S_z = -2$ states now favors the intermediate excited states having $S = 2$. Accordingly, Fig. 5(c) shows that in the asymmetric configuration $B_{\rm in}$ the occupation of the state with $S_z = 2$ already exceeds $P_{0,0}$ and $P_{1,0}$ around $t \sim 3.5$ ns. The stationary weight of the states $S_z = 0, \pm 2$ is quite similar to the one in Fig. 5(a). Similar considerations can be made when comparing the configuration $B_{\rm out}$ for the two resonant paths. We find in particular that the order in which $P_{0,0}$ and $P_{1,0}$ appear in the dynamics is reversed with respect to the configurations $B_{\rm in}$ and $B_{\rm sym}$. This happens because the vibrons are first generated in the "empty" states $|\phi_{0,-2}; N\rangle$.

We conclude our analysis by considering the effect of the transverse anisotropy on the dynamics of the molecular spin. To this end we performed transport calculations for several

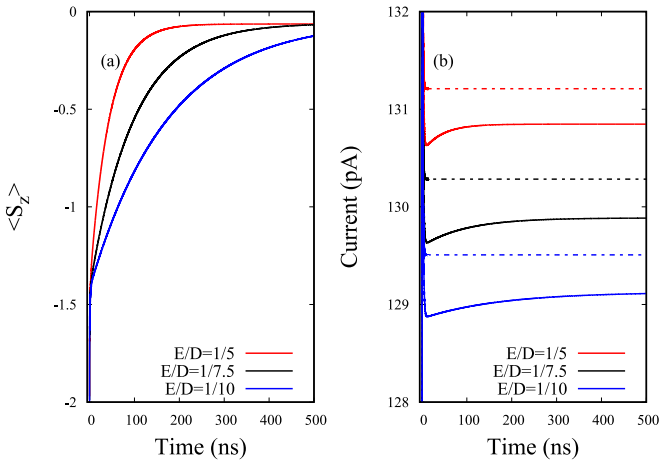

FIG. 6. (a) Average molecular spin for different values of the ratio E/D. (b) The time-dependent current J_R. The solid lines correspond to the spin-vibron coupling $\alpha = 0.15$ and the dashed lines to the noninteracting case $\alpha = 0$. The system is in the asymmetric bias configuration B_{in} at frequency $\omega_0 = \omega_-$.

lower values of the ratio E/D, by decreasing the transverse anisotropy coefficient E while keeping $D = 0.056$ meV. The slight change of the resonant frequencies $\omega_\pm$ as the transverse anisotropy varies was taken into account in order to ensure the resonant condition; that is, for each value of E/D we set $\omega_0 = \omega_-$. Because the spin-vibron coupling is directly proportional to E we recover again Rabi oscillations of the average spin, current, and vibron number in the short time regime (not shown). A more important effect of the transverse anisotropy is noticed in the intermediate and long-time spin dynamics.

In Fig. 6(a) one sees that as the ratio E/D decreases the stationary regime is reached at longer times (e.g., at $t \sim 400$ ns for $E/D = 1/7.5$). This is the expected behavior, given the fact that a smaller spin-vibron coupling leads to less effective off-resonant transitions between pairs of states carrying spin quantum number $S_z = 0$ and $S_z = 2$, whereas the resonant transitions between the states $S_z = 0, -2$ remain active.

In Fig. 6(b) we also identify small but systematic signatures of the spin-vibron coupling on the time-dependent output current J_R. More precisely, we compare the fully interacting currents corresponding to the three ratios E/D considered before and the noninteracting currents (i.e., in the absence of the spin-vibron coupling, $\alpha = 0$). In the latter case all currents display a sharp peak once the leads are coupled to the hybrid system and then decrease uniformly to the steady-state values [see the dashed lines in Fig. 6(b)]. In contrast, for $\alpha = 0.15$ (solid lines) one notices a nonmonotonous behavior, namely the sharp peak is followed by a slow but noticeable *increase* of J_R as it slowly approaches the steady-state value. The time range on which this smooth increase appears becomes longer if the ratio E/D decreases and roughly corresponds to the slower off-resonant spin dynamics shown in Fig. 6(a). Also, the steady-state values of the currents are slightly reduced in the presence of the spin-vibron coupling.

The specific values of the parameters ω, λ, T, and B used in our numerical simulations are of the same order of magnitude as the ones used in the experiment of Ganzhorn *et al.* [20]. The value $\hbar\omega_- = 0.27$ meV is within the range of the observed longitudinal stretching modes (see, for example, Ref. [22]). The correspondence between the electron-vibron coupling strength λ used in Eq. (5) and the measured dimensionless parameter g is given by the identity $g = (\lambda/\hbar\omega_0)^2$. For our values $\hbar\omega_- = 0.27$ meV and $\lambda = 0.2$ meV we get $g \approx 0.55$, which is consistent with the experimental data of Ganzhorn *et al.*

We stress that the *intrinsic* electron-vibron coupling in suspended carbon nanotubes is due to (i) the deformation potential associated with breathing or stretching modes and (ii) to the distortion-induced modification of bond lengths in the honeycomb lattice submitted to twist modes. Both mechanisms were discussed in detail in the theoretical work of Mariani and von Oppen [40]. From the Anderson-Holstein Hamiltonian describing the suspended CNT one identifies the electron-vibron coupling constant as an energy shift which depends on the deformation potential. The latter is calculated from the elastic theory of long-wavelength phonons.

The rather small value of the spin-vibron coupling reported in Ref. [20] ($g_{\text{s-ph}} = 1.5$ MHz) corresponds to the specific $S = 6$ TbPc2 molecule. For the simpler molecule of spin $S = 2$ considered in our work we assumed larger values (a typical matrix element of the spin-vibron coupling is around 50 MHz). Such values could be obtained for lighter nanomagnets. Nonetheless, the electron-vibron coupling strength λ dominates over the spin-vibron coupling. Our choice does not affect the results from the qualitative point of view.

Finally, let us emphasize that the prediction of Rabi oscillations in the transient regime discussed here might prove useful in future experiments as an indirect reading of resonant vibron-assisted transitions. In fact, one can switch between the two "paths" of the Λ configuration by adjusting the magnetic field such that Eq. (25) holds for one of the frequencies $\omega_\pm$.

Let us note that the amplitude of the currents depends on the frequency of the nanoresonator, as seen from the exponential term in the Lang-Firsov transform of the tunneling Hamiltonian. On the other hand, we find that the Lang-Firsov shifts $\lambda^2/\hbar\omega_0$ of the "bare" single-particle energy ϵ_0 differ by only 50 μeV and that the "ladder" of states $\mathcal{E}_{p,S_v,N}$ which contribute to the transport is not significantly altered when changing the frequency from ω_- to ω_+. Therefore, one can safely use the same bias window for both resonant paths.

IV. CONCLUSIONS

In this work we considered the electronic transport through a suspended nanosystem carrying a rigidly attached nanomagnet. Using a Markovian master equation we analyze the cumulative effects of both the electron-vibron and spin-vibron interactions. For suitable bias configurations the former allows vibron emission via electronic tunneling-in or -out processes, whereas the latter induces transitions of the localized spin. The molecular spin dynamics displays two time scales which are correlated to the Λ-type spectral structure of the hybrid system. The fast dynamics is associated to resonant transitions, while the much slower dynamics is due to slightly detuned transitions. Due to the spin-vibron coupling the molecular spin components of the hybrid system are mixed.

We find that the bias applied on the suspended structure sets the steady-state weights of the spin components for the grafted SMM.

Our numerical simulations also confirm that the spin-vibron coupling changes the transport properties of the hybrid system. In particular, we predict the existence of vibronic Rabi oscillations in the transient regime. Nonetheless, the effect of resonant and off-resonant vibron-assisted transitions of the spin states is difficult to predict or explain by inspecting or measuring the steady-state currents alone. To this end, the analysis presented in this work on the spin dynamics and on its correlation to the populations of various configurations of the hybrid system might prove useful for future experimental investigations.

ACKNOWLEDGMENTS

The authors acknowledge financial support from the Romanian Core Program PN19-03 (Contract No. 21 N/08.02.2019).

[1] D. Gatteschi, R. Sessoli, and J. Villain, *Molecular Nanomagnets* (Oxford University Press, Oxford, 2006).
[2] *Molecular Magnets*, NanoScience and Technology, edited by J. Bartolomé, F. Luis Julio, and F. Fernández (Springer, New York, 2014).
[3] L. Thomas, F. Lionti, R. Ballou, D. Gatteschi, R. Sessoli, and B. Barbara, Nature (London) **383**, 145 (1996).
[4] J. F. Nossa, M. F. Islam, C. M. Canali, and M. R. Pederson, Phys. Rev. B **88**, 224423 (2013).
[5] T. Komeda, H. Isshiki, J. Liu, Y.-F. Zhang, N. Lorente, K. Katoh, B. K. Breedlove, and M. Yamashita, Nat. Commun. **2**, 217 (2011).
[6] E. Burzurí, Y. Yamamoto, M. Warnock, X. Zhong, K. Park, A. Cornia, and H. S. J. van der Zant, Nano Lett. **14**, 3191 (2014).
[7] A. McCaskey, Y. Yamamoto, M. Warnock, E. Burzurí, H. S. J. van der Zant, and K. Park, Phys. Rev. B **91**, 125419 (2015).
[8] A. S. Zyazin, J. W. G. van den Berg, E. A. Osorio, H. S. J. van der Zant, N. P. Konstantinidis, M. Leijnse, M. R. Wegewijs, F. May, W. Hofstetter, C. Danieli, and A. Cornia, Nano Lett. **10**, 3307 (2010).
[9] M. Misiorny, E. Burzurí, R. Gaudenzi, K. Park, M. Leijnse, M. R. Wegewijs, J. Paaske, A. Cornia, and H. S. J. van der Zant, Phys. Rev. B **91**, 035442 (2015).
[10] C. Timm and F. Elste, Phys. Rev. B **73**, 235304 (2006).
[11] M. Misiorny and J. Barnaś, Phys. Rev. B **76**, 054448 (2007).
[12] V. Moldoveanu, I. V. Dinu, B. Tanatar, and C. P. Moca, New J. Phys. **17**, 083020 (2015).
[13] S. Zippilli, G. Morigi, and A. Bachtold, Phys. Rev. Lett. **102**, 096804 (2009).
[14] S. Zippilli, A. Bachtold, and G. Morigi, Phys. Rev. B **81**, 205408 (2010).
[15] M. Urdampilleta, S. Klyatskaya, J.-P. Cleuziou, M. Ruben, and W. Wernsdorfer, Nat. Mater. **10**, 502 (2011).
[16] I. V. Krainov, J. Klier, A. P. Dmitriev, S. Klyatskaya, M. Ruben, W. Wernsdorfer, and I. V. Gornyi, ACS Nano **11**, 6868 (2017).
[17] E. M. Chudnovsky, D. A. Garanin, and R. Schilling, Phys. Rev. B **72**, 094426 (2005).
[18] G. A. Steele, A. K. Hüttel, B. Witkamp, M. Poot, H. B. Meerwaldt, L. P. Kouwenhoven, and H. S. J. van der Zant, Science **325**, 1103 (2009).
[19] B. Lassagne, Y. Tarakanov, J. Kinaret, D. Garcia-Sanchez, and A. Bachtold, Science **325**, 1107 (2009).
[20] M. Ganzhorn, S. Klyatskaya, M. Ruben, and W. Wernsdorfer, Nat. Nanotechnol. **8**, 165 (2013).
[21] M. Ganzhorn, S. Klyatskaya, M. Ruben, and W. Wernsdorfer, Nat. Commun. **7**, 11443 (2016).
[22] S. Sapmaz, P. Jarillo-Herrero, Ya. M. Blanter, C. Dekker, and H. S. J. van der Zant, Phys. Rev. Lett. **96**, 026801 (2006).
[23] A. K. Hüttel, M. Poot, B. Witkamp, and H. S. J. van der Zant, New J. Phys. **10**, 095003 (2008).
[24] A. Benyamini, A. Hamo, S. V. Kusminskiy, F. von Oppen, and S. Ilani, Nat. Phys. **10**, 151 (2014).
[25] P. Weber, H. L. Calvo, J. Bohle, K. Gos, C. Meyer, M. R. Wegewijs, and C. Stampfer, Nano Lett. **15**, 4417 (2015).
[26] A. Einstein and W. J. de Haas, K. Akad. Wet. Amsterdam, Proc. **18**, 696 (1915).
[27] E. M. Chudnovsky and D. A. Garanin, Phys. Rev. B **81**, 214423 (2010).
[28] R. Jaafar, E. M. Chudnovsky, and D. A. Garanin, Europhys. Lett. **89**, 27001 (2010).
[29] M. F. O'Keeffe, E. M. Chudnovsky, and D. A. Garanin, J. Magn. Magn. Mater. **324**, 2871 (2012).
[30] D. A. Garanin and E. M. Chudnovsky, Phys. Rev. B **92**, 024421 (2015).
[31] D. A. Garanin and E. M. Chudnovsky, Phys. Rev. X **1**, 011005 (2011).
[32] F. May, M. R. Wegewijs, and W. Hofstetter, Beilstein J. Nanotechnol. **2**, 693 (2011).
[33] J. Brüggemann, S. Weiss, P. Nalbach, and M. Thorwart, Phys. Rev. Lett. **113**, 076602 (2014).
[34] A. Kenawy, J. Splettstoesser, and M. Misiorny, Phys. Rev. B **97**, 235441 (2018).
[35] M. F. O'Keeffe, E. M. Chudnovsky, and D. A. Garanin, Phys. Rev. B **87**, 174418 (2013).
[36] D. W. Utami, H.-S. Goan, and G. J. Milburn, Phys. Rev. B **70**, 075303 (2004).
[37] M. O. Scully and M. S. Zubairy, *Quantum Optics* (Cambridge University Press, Cambridge, UK, 1997).
[38] R. Dragomir, V. Moldoveanu, S. Stanciu, and B. Tanatar, Phys. Rev. B **101**, 165409 (2020).
[39] P. Meystre and M. Sargent, *Elements of Quantum Optics* (Springer, New York, 2007).
[40] E. Mariani and F. von Oppen, Phys. Rev. B **80**, 155411 (2009).